JOC The Journal of Organic Chemistry

Article

pubs.acs.org/joc

Axial Chirality of 4-Arylpyrazolo[3,4-*b*]pyridines. Conformational Analysis and Absolute Configuration

Pethaiah Gunasekaran,[†] Subbu Perumal,*[,†] J. Carlos Menéndez,[‡] Michele Mancinelli,[§] Silvia Ranieri,[§] and Andrea Mazzanti*[,§]

[†]Department of Organic Chemistry, School of Chemistry, Madurai Kamaraj University, Madurai 625 021, Tamil Nadu, India

[‡]Departamento de Química Orgánica y Farmacéutica, Facultad de Farmacia, Universidad Complutense, 28040 Madrid, Spain

[§]Department of Industrial Chemistry "Toso Montanari", University of Bologna, Viale Risorgimento 4, 40136 Bologna, Italy

Supporting Information

ABSTRACT: The stereodynamic behavior of a series of pyrazolo[3,4-*b*]pyridines was studied. The restricted rotations of the aryl substituent in position 4 of the heteroaromatic ring and of the benzoyl group in position 5 generated conformational enantiomers or conformational diastereoisomers depending on the local symmetry of the aryl substituent, with very high rotational barriers despite the absence of ortho-substituents. The energy barriers for the rotation of the 5-benzoyl group and the 4-aromatic ring were measured by dynamic NMR and rationalized by DFT calculations. When the aryl substituent at position 4 was 1-naphthyl, the resulting atropisomeric pair was resolved by means of enantioselective HPLC and the absolute configuration was determined by TD-DFT simulations of electronic circular dichroism spectra.

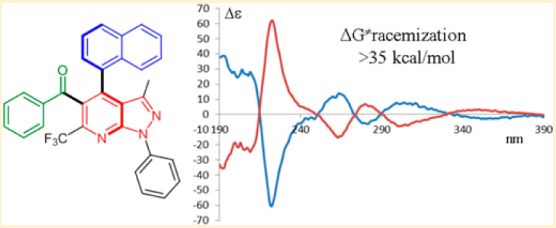

INTRODUCTION

When two aryl groups are bonded to the peri positions of a planar aromatic framework, they usually adopt a face to face (stacked) arrangement and display restricted rotation about the aryl−aryl bond. In particular cases, they might have a sufficiently high barrier as to produce configurationally stable stereoisomers.[1] A number of barriers for the interconversion of these isomers have been reported.[2] When the aryl substituents are not sufficiently large, stereolabile isomers (conformers) have often been observed and the corresponding interconversion barriers have been determined by variable temperature NMR spectroscopy.[3] Also heterocyclic rings bonded to the 1,8 positions of naphthalene displayed analogous features,[4] and similar barriers were also determined in the case of aryl groups bound onto other rigid frameworks such as anthracene,[5] biphenylene,[6] cyclobutane,[7] and acenaphthene.[8]

Likewise, the occurrence of two acyl groups in a peri relationship originates analogous stereolabile diastereoisomers because the same type of orthogonal conformation is adopted; the corresponding naphthyl−CO rotation barriers are lower than those found for aryl−aryl bonds and encompassing the 6.7−14.6 kcal/mol range.[9,10] As a consequence, when the same planar scaffold bears one acyl and one aryl substituent in a peri relationship, the two possible stereogenic axes might create either a pair of stereolabile enantiomers or diastereoisomers, depending on the symmetry of the aryl substituent.[11]

The pyrazolo[3,4-*b*]pyridine ring system has emerged as a privileged substructure in the pharmaceutical industry because of its occurrence in various biologically active compounds[12] exhibiting diverse medicinal properties,[13] and also act as vasodilators,[14] cyclin dependent kinase 1 inhibitors,[15] HIV reverse transcriptase inhibitors,[16] and protein kinase inhibitors.[17] Furthermore, pyrazolo[3,4-*b*]pyridines viz. cartazolate, etazolate, and tracazolate (Scheme 1), are well-established anxiolytic drugs.[18] Other pyrazolo[3,4-*b*]pyridine-containing bioactive compounds include a GSK-3 inhibitor and BAY 41-2272, a cardiovascular therapeutic agent and effective candidate in the treatment of Alzheimer's disease, respectively.[19] In addition to their pharmacological importance, pyrazolo[3,4-*b*]pyridines possess a high structural similitude to purine bases,

Scheme 1. Pyrazolopyridine-Embedded Drugs and Bioactive Compounds

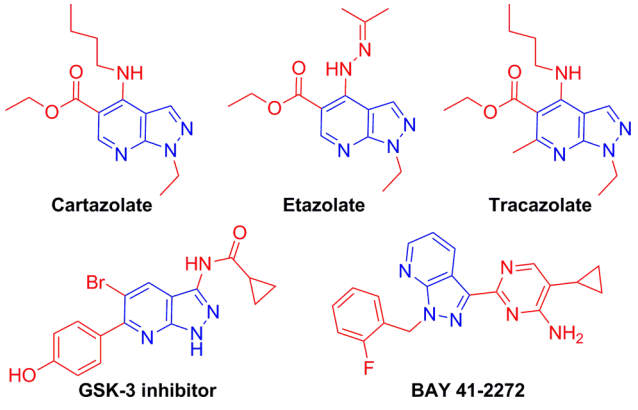

Received: September 4, 2014
Published: October 20, 2014

   dx.doi.org/10.1021/jo502047n | J. Org. Chem. 2014, 79, 11039−11050

essential constituents of DNA and RNA nucleosides,[20] which adds further significance to the synthesis and study of this moiety.

The aim of this paper is a thorough investigation of the stereodynamics of a class of pyrazolo[3,4-*b*]pyridines and an evaluation of the steric requirements needed to produce stable heteroaromatic atropisomers.[21] Atropisomerism has been heretofore largely overlooked as a source of stereoisomerism alternative to stereogenic centers. However, this situation changed with the discovery of many bioactive natural compounds containing stereogenic axes[22] and with the development of many approaches useful for their asymmetric synthesis.[23] Clayden, La Plante, and co-workers have recently begun to address the pharmaceutical implications of atropisomerism in drug discovery.[24−26] As an additional feature of interest, these compounds bear a fluorinated substituent on the heterocyclic scaffold. Over the years, a great deal of attention has been focused on the design and synthesis of fluorinated organic compounds because of their unique chemical and biological properties.[27] In particular, fluorine-containing building blocks have gained significant importance,[28] as synthons in the assembly of heterocycles,[29] in view of their remarkable applications in medicinal and agricultural fields.[30]

RESULTS AND DISCUSSION

The pyrazolo[3,4-*b*]pyridine scaffold of compounds **1**−**6** (Scheme 2) bears a methyl group in position 3 and a trifluoromethyl group in position 6. Both the aryl rings in position 4 and the benzoyl group in position 5 are therefore surrounded by sterically demanding nearby groups.

Scheme 2. Chemical Structure of Compounds 1−6

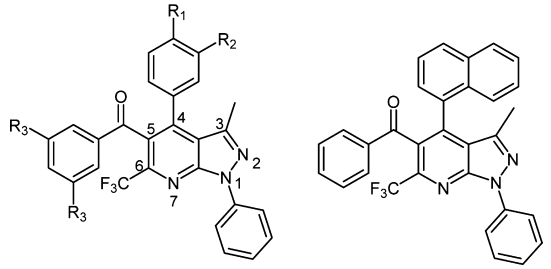

1 R_1 = OMe, R_2 = H, R_3 = H
2 R_1 = Me, R_2 = H, R_3 = H
3 R_1 = H, R_2 = Et, R_3 = H
4 R_1 = H, R_2 = *i*-Pr, R_3 = H
5 R_1 = H, R_2 = *i*-Pr, R_3 = Me

6

From a stereochemical point of view, compounds **1** and **2** bear a single stereogenic axis corresponding to the bond between the carbon in position 5 of the pyrazolo[3,4-*b*]pyridine and the benzoyl moiety. If the rotation around this axis is frozen in the NMR time scale, a pair of conformational enantiomers is generated (see Scheme 3). When optimized at the B3LYP/6-31G(d) level, the ground-state structures showed that the *p*-anisole ring in **1** (or *p*-tolyl in **2**) was almost perpendicular to the pyrazolo[3,4-*b*]pyridine ring, and the CO-Ph moiety was disposed in a skewed conformation, too. In its ground-state geometry, compounds **1** and **2** belong to the C_1 symmetry point group. These calculated structures fully agree with the known X-ray structure of compound **2**.[31]

Two transition states (TS-1 and TS-2 in Figure 1) should be considered to achieve racemization by the 180° rotation of the benzoyl moiety in compound **1**. In TS-1 the carbonyl oxygen

Scheme 3. The Two Enantiomeric Conformations of 1 and 2[a]

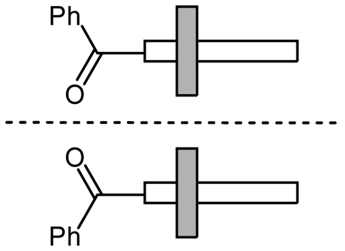

[a]The para-substituted phenyl moiety is sketched as a grey rectangle, while the white rectangle corresponds to the heterocyclic scaffold.

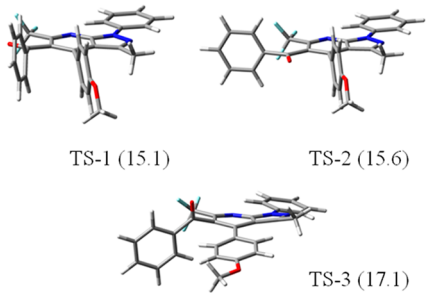

Figure 1. Calculated transition states for compound **1** at the B3LYP/6-31G(d) level. The reported energy values (in parentheses, relative to the ground state) are thermal corrected enthalpies, in kcal/mol.

crosses the pyrazolopyridine plane on the side of the trifluormethyl group, while in TS-2 the oxygen is close to the *p*-anisole group. According to DFT calculations, the transition state with the lower energy is TS-1, with a $\Delta H^{\ddagger}$ of 15.1 kcal/mol, while TS-2 has a $\Delta H^{\ddagger}$ of 15.6 kcal/mol. The computed transition state for anisole rotation corresponds to a coplanar conformation (TS-3 in Figure 1), and its energy was calculated as 17.1 kcal/mol.

The room temperature NMR spectrum of **1** showed some very broad peaks in the aromatic region, corresponding to the signals of the *p*-anisole ring. On raising the temperature above +25 °C, the broad signals sharpened at +93 °C into the expected AA′BB′ spectrum. On lowering the temperature, these signals sharpened and eventually split at −22 °C into two sets of signals in a 50:50 ratio (see Figure 2). The same behavior was observed in the case of compound **2** (see Figure S1 of Supporting Information (SI)). The experimental energy barriers were determined by line-shape simulations as 14.3 ± 0.2 kcal/mol and 14.1 ± 0.2 for **1** and **2**, respectively. The observed splitting of the aromatic hydrogens implies that the two sides of *p*-anisole (and *p*-tolyl as well) experience different magnetic environments. If the rotation of anisole is frozen and the benzoyl rotation is still fast in the NMR time scale, the two sides of anisole are enantiotopic; thus, their hydrogens are not anisochronous. If, on the contrary, the benzoyl rotation is frozen and the anisole rotation is fast, the two sides of anisole are exchanged by rotation (homomerization), and again no splitting is observed in the NMR spectrum. Nevertheless, the two sides of the aromatic ring belong to different magnetic environments when *both* rotations are frozen. For these reasons, the experimental energy barrier must be assigned to the lower calculated barrier for the two stereodynamic pathways, i.e., that for the benzoyl group rotation (calcd

dx.doi.org/10.1021/jo502047n | J. Org. Chem. 2014, 79, 11039−11050

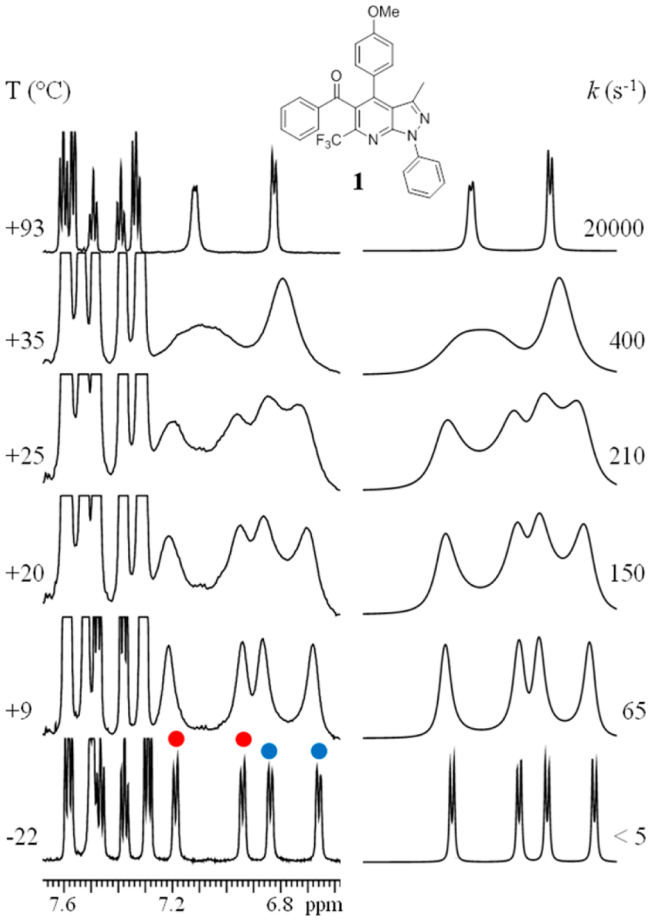

Figure 2. Left: temperature dependence of the ^{1}H aromatic signals of **1** (600 MHz in $C_2D_2Cl_4$). Right: line-shape simulations obtained with the rate constants reported. Blue dots indicate the hydrogens ortho to the methoxy group, and red dots indicate the hydrogens meta to the methoxy.

value 15.1 kcal/mol), while the energy barrier for the anisole rotation cannot be determined.

To get information about the stereodynamics of the aryl ring in position 4, we prepared compounds **3** and **4**. These bear in position 4 of the pyrazolo[3,4-*b*]pyridine core a *m*-ethylphenyl and a *m*-isopropylphenyl ring, respectively. The presence of a substituent in the meta position does not alter to a great extent the heteroaryl−aryl rotational barrier; nevertheless, the aromatic ring loses its local C_2 symmetry axis, and a new stereogenic axis is generated when its rotation is frozen. The ethyl and isopropyl groups were chosen because they act as stereochemical probes by showing diastereotopic signals in the NMR spectra.[32] The presence of a second stereogenic axis in addition to the benzoyl−heterocycle axis raises the number of conformations to be considered to four (see Scheme 4). When the dynamic process with the higher barrier is frozen, a pair of conformational enantiomers is generated, whereas when rotation around the second stereogenic axis is restricted, two pairs of conformational diastereoisomers are formed. If the meta substituent of the 4-phenyl ring (ethyl or isopropyl) and the oxygen of the benzoyl moiety are on the same side with respect to the plane of the pyrazolo[3,4-*b*]pyridine ring a syn diastereoisomer is generated, whereas in the anti conformational diastereoisomer the meta substituent and the oxygen lie on opposite sides of the heterocyclic plane. If the *M*, *P* descriptors are used for the two stereogenic axes,[33] the syn diastereoisomer corresponds to the 4*M**, 5*M** and the anti diastereoisomer to the 4*M**, 5*P** relative configuration, respectively.

Compound **3** crystallized as a racemate in the *P*-1 point group (see SI for details). The experimental structure (top of Figure 3) confirmed that the *m*-ethylphenyl and the CO moieties are skewed with respect to the pyrazolo[3,4-*b*]pyridine ring with interplanar angles of 61.7° and 71.6°, respectively. The conformation in the solid state has the CO and the *m*-ethyl group on the same side of the plane of the pyrazolo[3,4-*b*]pyridine scaffold, thus adopting a syn conformation.

Scheme 4. Stereochemical Pathways for Compounds 3−6[a]

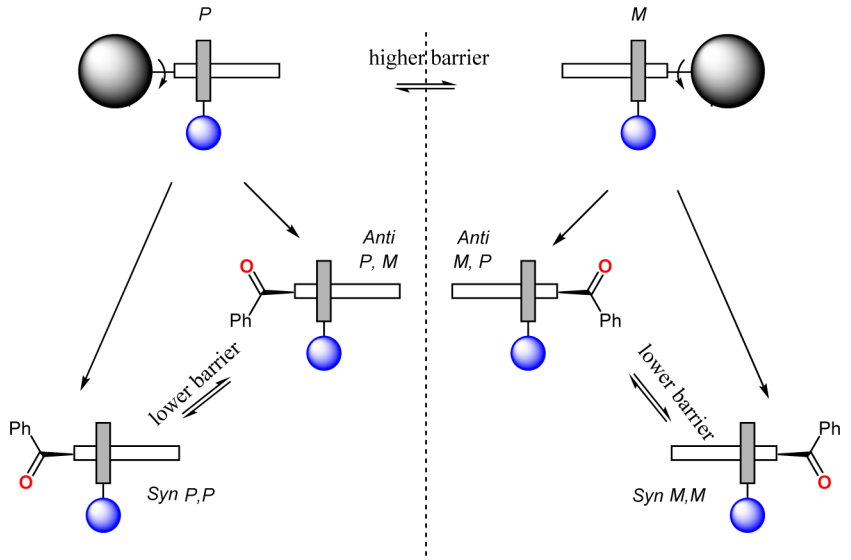

[a]The black spheres correspond to the benzoyl moiety. The blue spheres correspond to the meta substituent on the aryl ring in position **4** of the pyrazolopyridine ring.

dx.doi.org/10.1021/jo502047n | *J. Org. Chem.* 2014, 79, 11039−11050

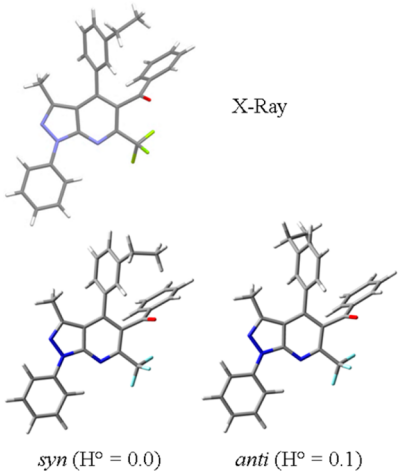

Figure 3. X-ray structure and DFT calculated structures for the two diastereoisomers of compound **3**. The reported energy values are thermal-corrected enthalpies, in kcal/mol.

The ethyl and isopropyl moieties should directly detect the conformational chirality by showing diastereotopic NMR signals for the two methylene protons of the ethyl moiety and for the two methyl groups of isopropyl (both in the ^{1}H and ^{13}C spectra). The formation of diastereoisomers can be detected by NMR at lower temperature by the formation of two sets of signals of different intensities. DFT calculations were performed to evaluate the energies of the two diastereoisomers of **3** and to pinpoint the transition states for the two stereodynamic pathways. The relative energies of the two diastereoisomers were computed at the B3LYP/6-31G(d) level, and they were found to be very similar (Figure 3). The syn conformer of **3** was the more stable by only 0.16 kcal/mol when the internal energy was considered, and by even less (0.10 kcal/mol) when the thermal-corrected enthalpy was taken into account.[34] The four conceivable transition states connecting the four conformations were calculated at the same level of theory (see Figure S2 of SI).

The rotation of the *m*-ethylphenyl ring comes across two transition states where the ethyl group points to either the methyl in position 3 of the pyrazolo[3,4-*b*]pyridine or the benzoyl group in position 5 (TS-3 and TS-4 in Figure S2 of SI). The rotation of the benzoyl moiety oversteps two transition states, where the CO is coplanar with the heterocyclic scaffold, and it is close either to the aryl ring in position 4 or to the CF_3 group in position 6 (TS-1 and TS-2 in Figure S2 of SI). For each rotational pathway, the lowest calculated energy barrier is the one to be considered for the comparison with experimental data. Calculated energies suggested that the rotation of the *m*-ethylphenyl group was again higher than that of the benzoyl group (18.1 and 14.9 kcal/mol, respectively).

The NMR spectrum of compound **3** recorded at room temperature showed broad peaks for both the CH_2 and CH_3 signals of the ethyl group. On lowering the temperature of a $C_2D_2Cl_4$ solution of **3**, the signals of the CH_2 decoalesced and eventually split into two quartets with 55:45 relative ratio at

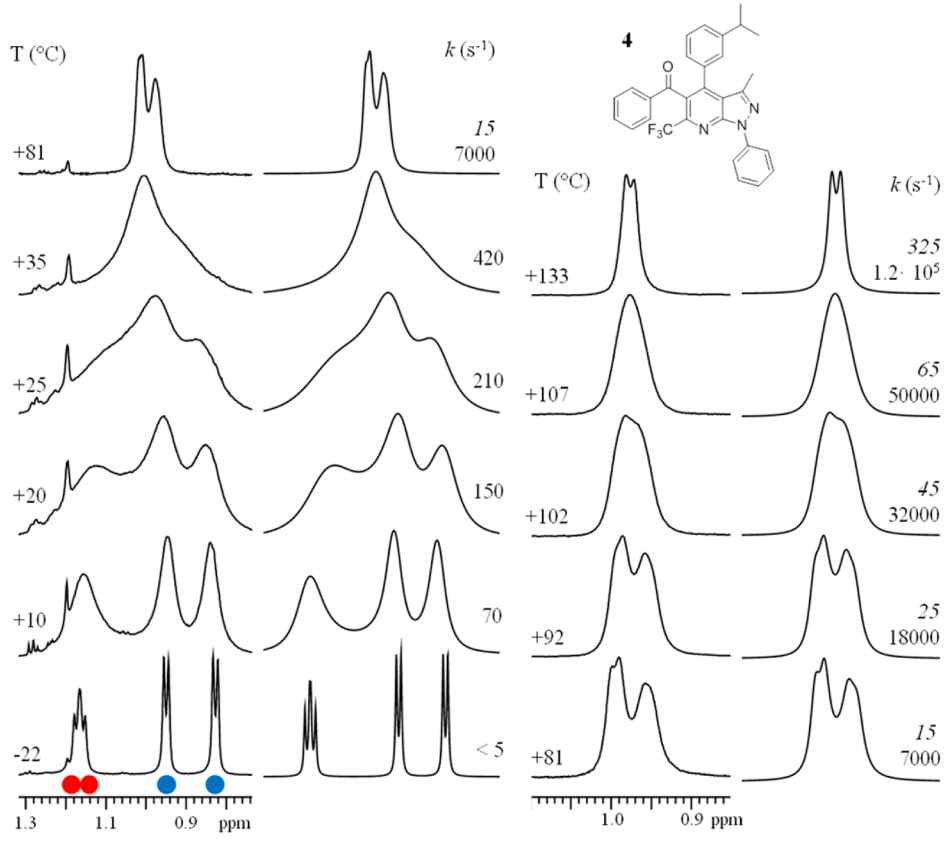

Figure 4. Temperature dependence of the ^{1}H NMR isopropyl methyl signal of **4** (600 MHz in $C_2D_2Cl_4$). Left: low-temperature part and corresponding line-shape simulations obtained with the rate constants reported. Right: high temperature spectra and line-shape simulations. Italicized rate constants are relative to the higher energy barrier, whereas the other rate constants are those for the lower barrier. The spectrum at +81 °C of the left side is the same at the bottom of the right side, where the chemical shift scale was expanded by a factor of **3**.

dx.doi.org/10.1021/jo502047n | J. Org. Chem. 2014, 79, 11039−11050

−22 °C (Figure S3 of SI). The unbalanced ratio confirmed that the two conformational diastereoisomers were present; thus, both rotational barriers must be frozen in the NMR time scale. The lack of diastereotopicity on the CH_2 signals is ascribable to a negligible chemical shift difference between the diastereotopic protons. The same signals did show diastereotopicity when acetonitrile-d_3 was used as solvent (Figure S4 of SI). Unfortunately, the low boiling point of the latter solvent did not allow the measurement of the higher of the two barriers. The diastereomerization barrier was conveniently measured by line-shape simulation of the methyl signal in $C_2D_2Cl_4$ (Figure S5 of SI), yielding a barrier of 13.9 ± 0.1_5 kcal/mol. Being the value identical (within the experimental errors) to that obtained for compounds **1** and **2**, this barrier should be again assigned to the benzoyl rotation, which also has the lower calculated barrier.

The measurement of the rotational barrier of the second stereogenic axis was accomplished with compound **4**, bearing a *m*-isopropylphenyl group. On lowering the temperature of a $C_2D_2Cl_4$ sample of **4**, the methyl signal split at −20 °C into three signals with 36:32:32 ratio (bottom trace of Figure 4) where the low field triplet (36%) is ascribable to the partial overlap of two doublets with the same intensity. Thus, in this compound the methyl groups of the isopropyl moiety display the expected diastereotopicity, and integration of the isopropyl CH signal confirmed the 64:36 ratio of the two conformational diastereoisomers. On raising the temperature, the broad signal observed at room temperature sharpened and two separated signals ($\Delta\nu$ = 21 Hz) were observed at +81 °C (top left trace of Figure 4). The two observed spectral lines correspond to the diastereotopic signals of the isopropyl group when the dynamic process with the lower barrier is fast in the NMR time scale, and the higher barrier process is still frozen (the coupling constant with the CH is still hidden within the line width).[35]

On further raising the temperature, the two signals reached coalescence at +102 °C, and a doublet due to the coupling with CH was eventually visible at +133 °C (right section of Figure 4). Two different sets of rate constants must be considered in the simulations. The first set accounts for the exchange between the pair of methyl signals of one diastereomeric conformation with the pair of methyl signals of the other. This rate constant corresponds indeed to the diastereomerization barrier and can be validated by the line-shape simulation of the CH signal, that is sensitive only to diastereomerization. The second set of rate constants must exchange the two diastereotopic methyl signals within the same diastereoisomer. The simulations displayed in the left section of Figure 4 correspond to the first set of rate constants that exchange the two more intense signals with the two less intense signals. The energy barrier derived from this simulation was 14.3 ± 0.1_5 kcal/mol, in good agreement with the values obtained for compounds **1**−**3**. In this temperature range the exchange rate between the diastereotopic signals within each conformation can be considered negligible. On the contrary, the simulations reported in the right side of Figure 4 must consider both rate constants. The rate constants for the lower-energy process were extrapolated at the requested temperature by keeping constant the $\Delta G^{\ddagger}$, whereas the second set of rate constants was optimized for the best simulation of the experimental line shape. The energy barrier derived for the higher energy process was 19.2 ± 0.2 kcal/mol. The experimental values have to be compared with the values of 15.6 and 18.4 kcal/mol provided by the calculations for the benzoyl and *m*-isopropylphenyl rotation, respectively. Again the trend and the values of the experimental barriers are well matched by DFT calculations.

To determine the structure of the more populated conformer of compounds **3** and **4**, NOE spectra were acquired. The spectra had to be recorded at a temperature (−67 °C) where the rotation of the benzoyl was calculated to have negligible rate (i.e., k < 0.01 s^{-1}), to avoid saturation transfer effects arising from the irradiated peak. Unfortunately, at this temperature the signals of the benzoyl moiety were heavily broadened by a third dynamic process (see below); thus, the NOE analysis was inapplicable. An approach based on the calculation of the NMR chemical shifts was applied to solve this dilemma. The NMR chemical shifts were calculated using the GIAO method at the B3LYP/6-311++G(2d,p)//B3LYP/6-31G(d) level on the two diastereomeric conformations. For both compounds **3** and **4**, the chemical shift calculations suggested that the major isomer has the anti conformation (full details and tables are reported in SI). With respect to **3**, the experimental diastereomeric ratio of **4** is more unbalanced (64:36 and 55:45 at −22 °C in $C_2D_2Cl_4$ for **4** and **3**, respectively). While the syn conformer was calculated to be slightly more stable than the anti conformer in compound **3**, in the case of **4** the anti conformational isomer was calculated as more stable than the syn conformational isomer, probably because of the larger steric hindrance of the isopropyl with respect to the ethyl group. This is therefore in agreement with the experimental trend.

As previously mentioned, below −60 °C the aromatic signals of the benzoyl moiety were heavily broadened by a third dynamic process. On lowering the temperature below −80 °C, the signal of the ortho hydrogens of the phenyl-CO ring reached coalescence and eventually split at −118 °C into two separated sets of signals in a 50:50 ratio (bottom trace of Figure S6 of SI). This third dynamic process has to be assigned to the restricted rotation of the phenyl ring around the C_{ipso}−CO bond. Due to the crowding of the aromatic region and to the large chemical shift spread, a complete line-shape simulation was not workable. An estimate of the barrier based on the coalescence temperature (about −80 °C) and on the chemical shift difference of the ortho signals yielded a value of 8.7 ± 0.3 kcal/mol. This value is larger than that measured for acetophenone itself (5.4 kcal/mol)[36] because in the present case the transition state, where the phenyl is perpendicular to the carbonyl moiety, is hindered by the presence of the aromatic ring in position 4 of the pyrazolopyridine and by the CF_3 in position 6. DFT calculations performed to simulate the rotational pathway of the phenyl group yielded a value of 9.9 and 10.1 kcal/mol for the syn and anti diastereoisomer, respectively, in fair agreement with the experimental values (Figure S7 of SI).

To monitor this barrier in a more accurate way and to have a complete line-shape simulation, we prepared compound **5** where the phenyl moiety was substituted with a 3,5-dimethylphenyl group. This chemical variation simplifies the aromatic region of the ^1H spectra, but it does not alter the rotational barrier of the phenyl ring, and the signals of the newly introduced methyl groups can be used for the line-shape simulation as well. For this compound, the barrier for the rotation of the *m*-isopropylphenyl ring and the diastereoisomerization barrier were found to be identical to those of compound **4** (19.2 kcal/mol ± 0.2 and 14.3 ± 0.2 kcal/mol, respectively). The diastereomeric ratio was 63:37 at −22 °C in $C_2D_2Cl_4$, see Figures S8 and S9 of SI). On lowering the

dx.doi.org/10.1021/jo502047n | J. Org. Chem. 2014, 79, 11039−11050

temperature below −80 °C, the two unbalanced signals of the CH_3 of the 3,5-dimethylphenyl group broadened and split into four separated peaks at −118 °C, due to the frozen rotation of the 3′,5′-dimethylphenyl ring (Figure S10 of SI). The line-shape simulations yielded two different rotational barriers (9.6 ± 0.2 and 9.4 ± 0.2 kcal/mol),[37] with the major diastereoisomer having the higher rotational barrier. Calculations suggested that the higher barrier is that of the anti diastereoisomer (10.4 vs 10.1 kcal/mol) because of the steric clash of the 3′ methyl with the phenyl in the transition state. This result further supports the hypothesis of a more populated anti diastereoisomer, as found for compound **4**. The experimental values of the energy barriers measured for all the studied compounds are reported in Table 1.

Table 1. Summary of the Syn:Anti Ratio and of the Experimental Energy Barriers for 4-Aryl Rotation and 5-Benzoyl Rotation[a]

compound	experimental syn:anti ratio	4-aryl rotation	5-benzoyl rotation
1	–	– (17.1)	14.3 (15.1)[b]
2	–	– (17.5)	14.1 (14.8)[b]
3	44:56 (−22 °C)	– (18.1)[b]	13.9 (14.9)[b]
4	36:64 (−22 °C)	19.2 (18.0)[b]	14.3 (14.7)[b]
5	37:63 (−22 °C)	19.2 (18.1)[b]	14.3 (14.9)[b]
6	38:62 (−35 °C)	>35 (36.4)[b]	13.0 (14.2)[b]

[a]In parentheses are reported the DFT calculated values at the B3LYP/6-31G(d) level, as thermal-corrected enthalpies. All the values are in kcal/mol. [b]The reported energy value is that of the lower energy transition state.

ATROPISOMER SEPARATION AND ABSOLUTE CONFIGURATION

Due to the steric constraints, the rotational barriers measured for the *m*-ethylphenyl and *m*-isopropylphenyl group in compounds **3** and **4** were very high, despite the substituents being in the meta position of the ring. For this reason, we speculated that a substituent in the ortho position of the aryl ring in position 4 of the pyrazolopyridine should provide a torsional barrier sufficiently high to allow for a physical resolution of the atropisomeric pair. We thus prepared compound **6** containing the 1-naphthyl ring, because DFT calculations suggested a rotational barrier exceeding 36 kcal/mol (see Figure S11 of SI for the TS geometry).

As the first step, we pursued the resolution of the atropisomeric pair by means of enantioselective HPLC on a chiral stationary phase. We found that an amylose-based stationary phase (Chiralpak AD-H) was able to separate the two atropisomers with good performance in terms of separation and retention times. A good amount of the two atropisomers were obtained by means of a semipreparative approach and the electronic circular dichroism (ECD) spectra recorded in acetonitrile showed the expected opposite traces (Figure 5). Being too high for the dynamic NMR approach, we tried to measure the racemization barrier by keeping an enantiopure sample of **6** at +120 °C for 24 h in 1,1,2,2-tetrachloroethane. Subsequent HPLC analysis did not show the presence of the second atropisomer, yet it showed the formation of some degradation products. Unfortunately, when heated to +146 °C (i.e., the boiling point of 1,1,2,2-tetrachloroethane), the compound was not thermally stable and only degradation products were detected. Assuming the second atropisomer to

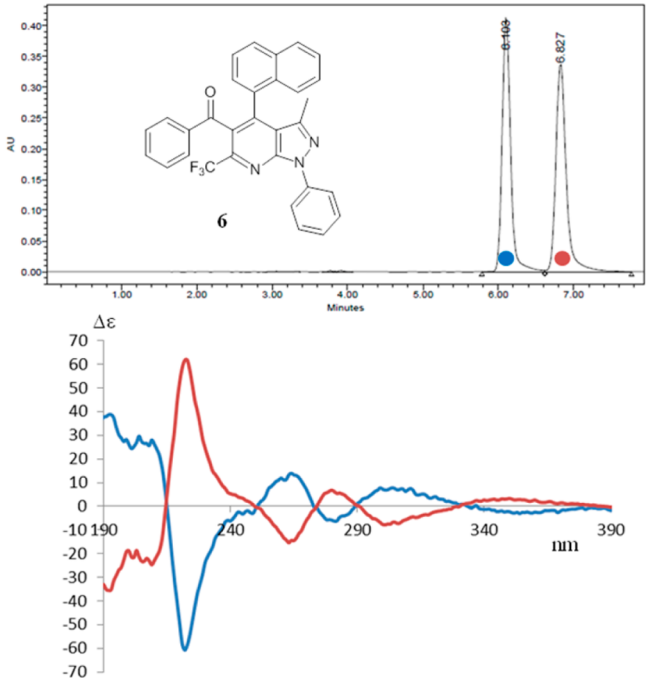

Figure 5. Top: HPLC chromatogram of **6** on chiral stationary phase (Chiralpak AD-H). Bottom: ECD spectra of the two atropisomers taken in acetonitrile solution.

be present as less than 1% after 24 h at +120 °C, the lower limit of the racemization barrier is about 35 kcal/mol, in good agreement with the DFT calculated value of 36.4 kcal/mol. This value corresponds to a "class 3" atropisomer in La Plante's scheme[25] with a half-life time of more than 2×10^5 years at ambient temperature.

The diastereoisomeric ratio at −35 °C was 62:38 in $C_2D_2Cl_4$, and line-shape simulation of the signal of the methyl in position 3 provided a value close to that of **1**−**5** for the benzoyl rotation (13.0 ± 0.2 kcal/mol, see Figure S12 of SI). Having in hand the two separated atropisomers of compound **6**, we pursued the determination of their absolute configuration. The reference method to assign the absolute configuration (AC) relies on the X-ray anomalous scattering[38] that in the present case would require high-quality single crystals and the use of a Cu−Kα X-ray source.[39,40] Nevertheless, the determination of the AC of chiral molecules by chiro-optical techniques such as optical rotation (OR), vibrational circular dichroism (VCD), and electronic circular dichroism (ECD) has recently gained feasibility and reliability thanks to the development of the time-dependent density functional theory approach (TD-DFT).[41]

The experimental ECD spectrum of compound **6** shows a rather complex pattern (the UV spectrum is shown in Figure S13 of SI). The typical features of the 1-naphthyl chromophore are found in the weak band at 285 nm and in the strong band at 225 nm.[42] These Cotton effects are due to the ^1L_a and ^1B_b transitions, polarized along the short and long axis of the naphthalene, respectively. The ECD spectrum also shows two Cotton effects at 266 and 308 nm and a weak band at 355 nm. The two bands related to the two transitions of acetophenone are found at 266 and 195 nm (polarized along the long and short axis, respectively).[43]

The electronic excitation energies and rotational strengths were calculated for the two conformational diastereoisomers in

dx.doi.org/10.1021/jo502047n | J. Org. Chem. 2014, 79, 11039−11050

the gas phase using the geometries optimized at the B3LYP/6-31G(d) level and using TD-DFT with four different functionals to explore whether different theoretical models provide different shapes of the simulated spectra. Simulations were performed by means of the hybrid functionals BH&HLYP[44] and M06-2X,[45] the long-range correlated ωB97XD that includes empirical dispersion,[46,47] and CAM-B3LYP that includes long-range correction using the Coulomb Attenuating Method.[48] Two explorative tests were performed using different basis sets that proved to be accurate for these calculations such as 6-311++G(2d,p)[49] and def2-TZVP[50] with the ωB97XD functional without appreciable differences (see Figure S15 of SI). An attempt was made also by including the solvent (acetonitrile) in the calculations using the PCM approach,[51] but no significant differences were observed. For these reasons, all the TD-DFT calculations employed the 6-311++G(2d,p) basis set and were performed without considering the solvent. As shown in Figure 6, the simulated

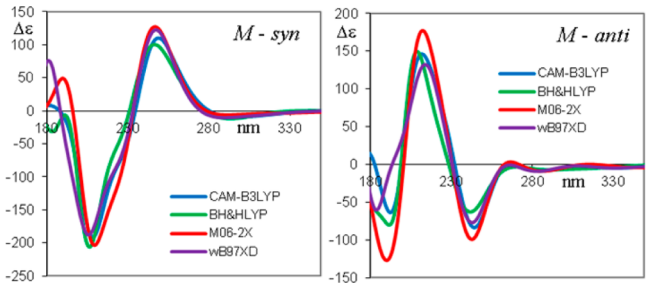

Figure 6. Theoretical ECD spectra of the two conformations of the *M* atropisomer of compound **6** calculated with TD-DFT and four different functionals with the 6-311++G(2d,p) basis set. All the spectra were obtained by applying Gaussian shapes (line width = 0.25 eV) to 60 discrete transitions.

ECD spectra for the anti and syn conformers of the *M* atropisomer are very similar within the same conformation, but nearly opposite spectra are generated for the two conformations. The averaged ECD spectrum will be therefore extremely sensitive to the population ratio.[49]

At first sight, it could seem odd that the ECD spectra of the two conformations are nearly opposite, because the stereogenic axis generated by the 1-naphthyl group and the heteroaromatic ring has the same configuration within the two conformational isomers, and the two dipoles oriented along the long axes of naphthalene and pyrazolopyridine were supposed to produce an exciton coupling easily understandable by considering the sign of the dihedral angle.[52] The reasons for the inversion of the spectrum must therefore be searched in the opposite disposition of the benzoyl group with respect to naphthalene in the two conformational diastereoisomers. The high-energy part of the spectrum (from 270 to 190 nm) can be interpreted as the result of the coupling of the naphthalene band at 225 nm with the two bands of benzoyl, that are known to have strong UV absorbance at 190−200 and 235 nm ($\varepsilon \approx 40\,000$ and 1500 in the gas phase[43]).

Considering the two bands calculated at 245 and 225 nm, that correspond to the transitions oriented on the long axis of benzoyl and on the long axis of naphthalene, the two dipoles form a positive dihedral angle in the syn conformation and negative in the anti (see Figure 7). When the higher energy band of benzoyl at 195 nm is considered, the dihedral angle with naphthalene is positive in the anti conformer and negative

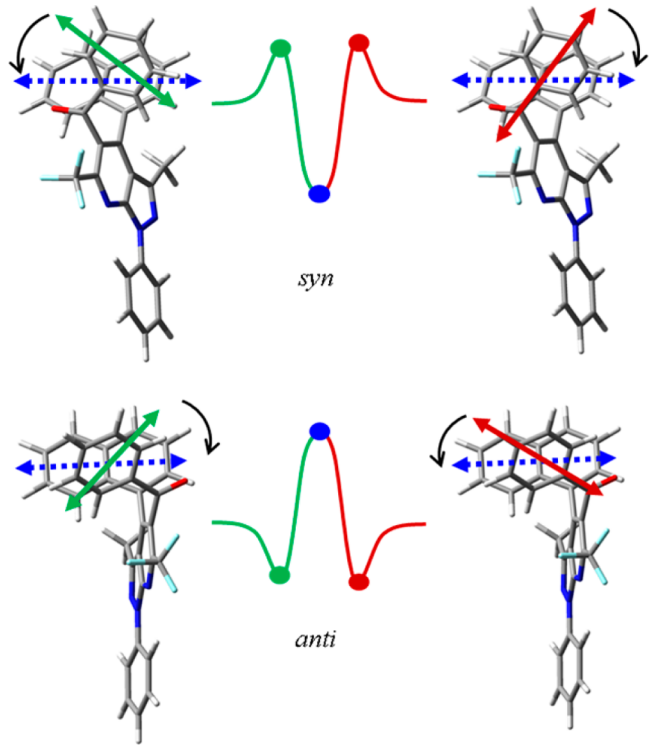

Figure 7. UV transitions yielding the high-energy part of the ECD spectrum of the syn and anti diastereoisomers of **6**. The blue dashed arrows, corresponding to the ^1B_b band of naphthalene, are always behind the two dipoles of benzoyl (red and green double arrows). In the middle are sketched the resulting ECD spectra.

in the syn. The combination of the two relative dispositions of the dipoles of benzoyl produces two opposite exciton couplings with the ^1B_b transition of naphthalene, thus yielding opposite patterns for the two conformations.

An investigation of the molecular orbitals (MO) involved in the UV transitions that generate these ECD bands confirmed that the band centered at 245 nm is mainly generated by MOs that involve the naphthalene and the CO-Ph group, with smaller contributions coming from MOs involving the *N*-phenyl ring and the pyrazolopyridine ring. The same happens in the high energy band at 190 nm generated by transitions related to the CO-phenyl ring and naphthalene (see Figures S16, S17, and Tables S4, S5 of SI). The experimental ECD spectrum being the weighted sum of the spectra of the diastereoisomers, the correct ratio must be used, at the expense of a wrong AC assignment. The NMR spectra taken at −30 °C in $C_2D_2Cl_4$ showed a ratio of 59:41 for the two conformational diastereoisomers, and the ratio was almost invariant when different solvents were used (61:39 in CD_3OD and 58:42 in CD_3CN). Unfortunately, NOE spectra were again thwarted by the slow rotation of the benzoyl moiety at the low temperatures required to make negligible the rate constant of the diastereomerization process. However, the X-ray structure of racemic **6** showed that the conformation present in the solid state was anti (Figure 8). This is in agreement with the results of DFT calculations that suggested the anti diastereoisomer to be more stable than the syn diastereoisomer, albeit by a small difference (0.35 kcal/mol at the B3LYP/6-31G(d) level). Inclusion of the solvent (methanol, PCM method) in the calculations led to a difference of 1.13 kcal/mol (as $\Delta H°$), whereas a different theoretical level [ωB97XD/6-311++G-

dx.doi.org/10.1021/jo502047n | J. Org. Chem. 2014, 79, 11039−11050

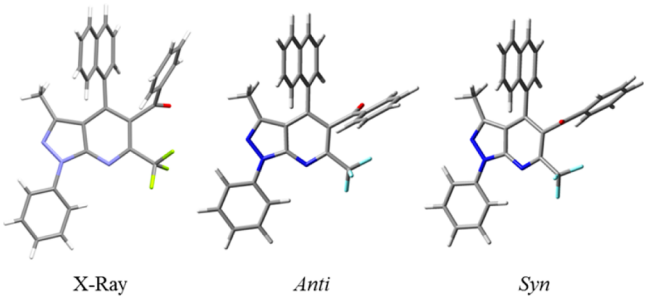

Figure 8. X-ray structure of racemic **6** and optimized structures for the two conformational diastereoisomers.

(2d,p)] yielded a difference of 1.7 kcal/mol. Although the conformation observed in the solid state usually corresponds to the more populated in solution, the small experimental difference in the population ratio in solution cannot rule out that the preference for the anti structure in the solid state could be ascribable to a more favorable crystal packing.

As for compounds **3** and **4** further information can be obtained by chemical shift calculations. The five experimental chemical shifts of the phenyl group observed at −95 °C are matched by the values calculated for the anti configuration, whereas the shifts calculated for the syn isomer are largely different (see Figure S18 of SI and related discussion). The coincidence of the solid-state structure, the chemical shift analysis, and the relative energies provided by calculations allowed us to safely assign the anti as the more populated isomer in solution. When the ratio provided by NMR was used to weight the ECD spectra of the two conformations, the resulting spectrum was in very good agreement with the experimental spectrum of the second eluted atropisomer of compound **6**, to which the *M* absolute configuration can be assigned (Figure 9 and Figure S19 of SI).

The best agreement with the experimental spectrum was obtained with the BH&HLYP and the ωB97XD functionals

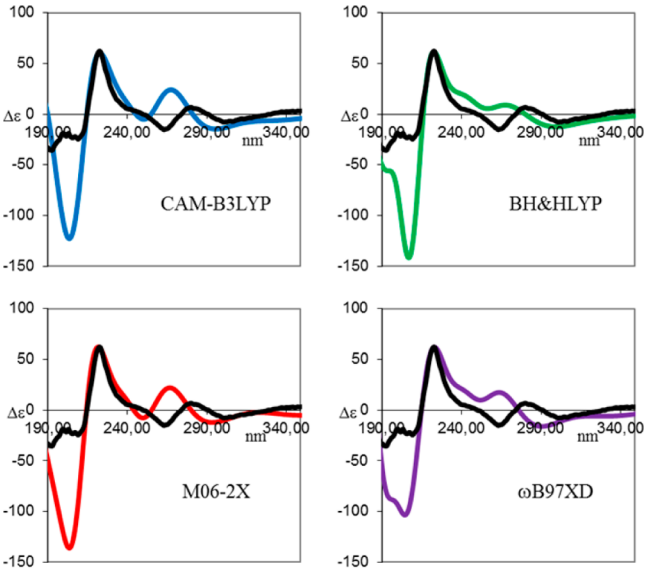

Figure 9. Colored lines: computed ECD spectra of the *M* atropisomer of **6** using different functionals and considering a 58:42 ratio of the two conformations (anti/syn). All the calculations employed the 6-311++G(2d,p) basis set. Black line: experimental ECD spectrum of the second eluted atropisomer of **6**.

when the simulated spectrum of the anti diastereoisomer was red-shifted by 6 nm with respect to that of the syn conformer. This could be ascribed to the different ability of the CO moiety to interact with the solvent (acetonitrile) in the two conformations. In the anti conformation the carbonyl group is more accessible to solvent, and $\pi \rightarrow \pi^*$ transitions are known to be shifted to longer wavelength in the presence of a polar solvent such as acetonitrile.[53]

CONCLUSIONS

In this work we have analyzed the stereodynamic behavior of a series of 4-aryl5-benzoyl-6-(trifluoromethyl)pyrazolo[3,4-*b*]-pyridine derivatives. The restricted rotations of the aryl substituent in position 4 of the heteroaromatic ring and of the benzoyl group in position 5 generate conformational enantiomers or conformational diastereoisomers depending on the local symmetry of the aryl ring in position 4. The energy barriers for the rotation of the benzoyl group and for the aromatic ring were measured by dynamic NMR and rationalized by DFT calculations. In all the analyzed compounds the 4-aryl rotation was found to have a larger barrier than the benzoyl rotation, and its value was found to be quite large, despite the absence of any ortho substituent on the aromatic ring. At very low temperatures (i.e., <−80 °C), a third dynamic process due to rotation around the phenyl−CO bond was observed. When the 4-aryl ring was the 1-naphthyl (compound **6**), the arene−heterocyclic ring rotational barrier was larger than 35 kcal/mol, and the atropisomeric pair was resolved by means of enantioselective HPLC. Also in this case the restricted rotation of the benzoyl group yielded two conformational diastereoisomers detectable with dynamic NMR. Using the experimentally determined ratio of the two conformational diastereoisomers, the absolute configuration of the atropisomers was determined by simulating the electronic circular dichroism spectra using TD-DFT calculations.

The synthesis and the chemistry of the pyrazolopyridine derivatives has attracted much attention in view of their importance as the core structure of numerous biologically active compounds. However, they are not intrinsically chiral, and classical sp^3 stereocenters can be added only far away from the heterocycle. The availability and synthetic feasibility of thermally stable heteroaryl−aryl atropisomers could spread and enhance the biological activity of these compounds thanks to the newly added stereogenic moiety, directly connected to the pyrazolopyridine core.

EXPERIMENTAL SECTION

Materials. Compounds **1** and **2** were known[31] and compounds **3**−**6** were prepared as reported in the literature.[31] *n*-Butyllithium (1.6 M in hexane), dimethylformamide, 4,4,4-trifluoroacetoacetic acid ethyl ester, 3-isopropylbenzaldeyde, 3,5-dimethylacetophenone, 5-amino-3-methyl-1-phenylpyrazole, and L-proline were commercially available. 1-(3,5-Dimethylphenyl)-4,4,4-trifluoro-1,3-butanedione was prepared according to the literature.[54] Diisopropylamine was freshly distilled from CaH_2 prior to use. Et_2O and THF were dried before use by distillation over Na/benzophenone. $CDFCl_2$ was prepared according to a known procedure.[55] The following stationary phases were employed for the chromatography: Silica gel 60 Å F254 (Merck) for the TLC and silica gel 60 Å (230−400 mesh, Sigma-Aldrich) for atmospheric pressure chromatography. Reactions that needed anhydrous conditions were performed under a dry nitrogen flow. The glassware used in these reactions was placed in an oven at +100 °C for at least 3 h immediately before use. Semipreparative enantioselective HPLC column (Daicel ChiralPak AD-H 250 × 20

dx.doi.org/10.1021/jo502047n | J. Org. Chem. 2014, 79, 11039−11050

mm) was used to obtain enantiomerically pure atropisomers of compound **6**.

Spectroscopic Data. NMR spectra were recorded using a spectrometer operating at a field of 14.4 T (600 MHz for ^{1}H, 150.8 for ^{13}C). ^{19}F NMR spectra were recorded using a spectrometer operating at a field of 9.4 T (376.3 MHz). Chemical shifts are given in ppm relative to the internal standard tetramethylsilane (^{1}H and ^{13}C) or relative to the residual peak of the solvents. ^{19}F chemical shift are given relative to the external standard $CFCl_3$. The assignment of the ^{13}C signals was obtained by means of DEPT, gs-HSQC, and gs-HMBC spectra. The 150.8 MHz ^{13}C NMR spectra were acquired under proton decoupling conditions with a 36 000 Hz spectral width, 5.5 μs (60° tip angle) pulse width, 1 s acquisition time, and 9 s delay time. The long relaxation time was needed to observe the CF_3 carbon and some quaternary carbons of the heterocycle. A line broadening function of 1−2 Hz was applied before the Fourier transformation. ^{1}H and ^{13}C NMR spectra for compound characterization were recorded at +50 °C to get sharper lines. The 376.3 MHz ^{19}F NMR spectra were acquired with a 75 200 Hz spectral width (200 ppm), 4.2 μs (30° tip angle) pulse width, 0.85 s acquisition time, and 1 s delay time. NOE spectra were obtained at 600 MHz using the DPFGSE sequence[56] and a 50 Hz wide selective pulse with a R-SNOB shape.[57]

Variable Temperature NMR. The low temperature NMR spectra were obtained by using a flow of dry nitrogen which entered into an inox steel heat exchanger immersed in liquid nitrogen and connected to the NMR probe head by a vacuum-insulated transfer line. The 600 MHz ^{1}H spectra were acquired using a 5 mm direct probe with a 9000 Hz spectral width, 2.0 μs (20° tip angle) pulse width, 3 s acquisition time, and 1 s delay time. A shifted sine bell weighting function equal to the acquisition time (i.e., 3 s) was applied before the Fourier transformation. Temperature calibrations were performed before the experiments, using a digital thermometer and a Cu/Ni thermocouple placed in an NMR tube filled with isopentane or 1,1,2,2-tetrachloroethane (for the low and high temperature range, respectively). The uncertainty in the temperature measurements can be estimated from the calibration curve as ±1 °C. Line-shape simulations were performed using a PC version of the QCPE DNMR6 program.[58] Electronic superimposition of the original and the simulated spectra enabled the determination of the most reliable rate constants at a few different temperatures. These constants provided the free energies of activation ($\Delta G^{\ddagger}$) by means of the Eyring equation. Within the experimental uncertainty, the latter values were found essentially invariant in the examined temperature range, thus implying an almost negligible activation entropy $\Delta S^{\ddagger}$.[59]

ECD Spectra. ECD spectra were recorded at +25 °C in far-UV HPLC-grade acetonitrile solutions. The concentrations of the samples (about 10^{-4} M) were tuned by dilution of a stock solution (1×10^{-3} M) to obtain a maximum absorbance of about 0.8 ÷ 0.9 in the UV spectrum using a 0.2 cm path length. The spectra were recorded in the 190−400 nm interval as the sum of 16 spectra. Reported $\Delta\varepsilon$ values are expressed as L mol^{-1} cm^{-1}.

Calculations. Ground-state optimizations and transition states were obtained by DFT computations performed by the Gaussian 09 rev A.02 series of programs[60] using standard parameters. The calculations for ground states and transition states employed the B3LYP hybrid HF-DFT functional[61] and the 6-31G(d) basis set. The analysis of the vibrational frequencies for the optimized structures showed the absence of imaginary frequencies for the ground states, and the presence of one imaginary frequency for each transition state. Visual inspection of the corresponding normal mode[62] validated the identification of the transition states. If not differently stated, the energy values presented in the Results and Discussion derive from total electronic energies. The ECD spectra of compound **6** were calculated using TD-DFT using BH&HLYP,[44] M06-2X,[45] ωB97XD,[46] CAM-B3LYP,[48] and the 6-311++G(2d,p) basis set. Sixty discrete transitions were calculated for each conformation (lowest calculated wavelength about 160 nm), and the ECD spectrum was obtained by convolution of Gaussian shaped lines (0.25 eV line width).[62] The simulated spectra resulting from the Boltzmann averaged sum of the conformations were red-shifted by 6−12 nm to get the best simulations with the experimental spectra.

4,4,4-Trifluoro-1-(3,5-dimethylphenyl)butane-1,3-dione (7). Prepared according to a known procedure.[54] Diisopropylamine (1.14 mL, 0.82 g, 8.1 mmol) was dissolved in 40 mL of THF. The solution was cooled to −20 °C, and then a solution of *n*-BuLi in hexane (1.6 M, 5 mL, 8 mmol) was added dropwise. The mixture was stirred for 30 min at −20 °C, and then the temperature was allowed to rise to +5 °C and then cooled down to −78 °C. A solution of 3,5-dimethylacetophenone (1.00 g, 6.7 mmol) was then added dropwise to the solution of LDA. The reaction mixture was stirred for 30 min at −78 °C, and its color went from colorless to yellow. A solution of 4,4,4-trifluoroacetoacetic acid ethyl ester (0.97 mL, 1.15 g, 8.1 mmol in 5 mL of THF) was added dropwise to the solution of enolate. The reaction was stirred at −78 °C for 1 h and then allowed to warm to ambient temperature overnight. Saturated NH_4Cl solution was then added, and the mixture was extracted with diethyl ether (3 × 30 mL). The combined organic layers were dried (Na_2SO_4), filtered, and concentrated under reduced pressure. The residue was purified by dissolving the impurities in $CHCl_3$ and by recrystallization from acetonitrile, yielding the title compound as a white solid (798 mg, 40%). mp +280 °C (decomp). ^{1}H NMR (600 MHz, CD_3CN, 1.96 ppm, +25 °C): δ 2.35 (s, 6H), 2.32 (s, OH), 6.23 (s, 1H), 7.15 (s, 1H), 7.51 (s, 2H). ^{13}C NMR (150.8 MHz, CD_3CN, 1.79 ppm, +25 °C): δ 21.8 (CH_3), 90.9 (CH), 121.1 (q, J = 279 Hz, CF_3), 126.4 (CH), 134.1 (Cq), 139.4 (CH), 172.4 (q, J = 35 Hz, CO-CF_3), 190.5 (CO). ^{19}F NMR (376 MHz, CD_3CN, +25 °C): δ −76.3 (s). HRMS (ESI-TOF-MS^-) m/z: $[M - H]^-$ calcd for $C_{12}H_{10}F_3O_2$: 243.06329; found: 243.06369.

General Procedure for the Synthesis of 3-Methyl-1-phenyl-1*H*-pyrazolo[3,4-*b*]pyridines 3−6. A mixture of 4,4,4-trifluoro-1-phenylbutane-1,3-dione (1 mmol), the appropriate aromatic aldehyde (1 mmol), 3-methyl-1-phenyl-1*H*-pyrazol-5-amine (1 mmol), and L-proline (0.20 mmol) in ethanol (15 mL) was stirred at +60 °C overnight. The reaction mixture was then extracted with ethyl acetate (2 × 40 mL), and after removal of the solvent, the crude was chromatographed over silica gel using petroleum ether−ethyl acetate mixture (4:1 v/v), which afforded pure compounds **3**, **4**, and **6**. 4,4,4-Trifluoro-1-(3,5-dimethylphenyl)butane-1,3-dione **7** (0.2 mmol), *m*-isopropylbenzaldehyde (0.2 mmol), 3-methyl-1-phenyl-1*H*-pyrazol-5-amine (0.2 mmol), and L-proline (0.05 mmol) in ethanol (5 mL) were used for the preparation of compound **5**.

4-(4-Methoxyphenyl)-(3-methyl-1-phenyl-6-(trifluoromethyl)-1*H*-pyrazolo[3,4-*b*]pyridine-5-yl)(phenyl)methanone (1).[31] Yield: 400 mg (82%, relative to *p*-methoxybenzaldehyde). White solid, mp 150−151 °C. ^{1}H NMR (600 MHz, CD_3CN, +50 °C): δ 2.11 (s, 3H), 3.77 (s, 3H), 6.85 (bs, 2H), 7.17 (d, J = 8.0 Hz, 2H), 7.37 (t, J = 7.9 Hz, 2H), 7.43 (t, J = 7.5 Hz, 1H), 7.55 (t, J = 7.5 Hz, 1H), 7.60−7.65 (m, 4H), 8.32 (d, J = 8.1 Hz, 2H). ^{13}C NMR (150.8 MHz, CD_3CN, +50 °C): δ 15.4 (CH_3), 56.7 (OCH_3), 115.0 (CH), 118.9 (Cq), 122.6 (CH), 123.4 (q, J = 275.4 Hz, CF_3), 126.9 (Cq), 128.1 (CH), 128.9 (Cq), 130.1 (CH), 130.9 (CH), 130.9 (CH), 132.8 (CH), 135.4 (CH), 139.2 (Cq),140.6 (Cq), 144.2 (q, J = 35.1 Hz, C-CF_3), 145.7 (Cq), 147.8 (Cq), 150.7 (Cq), 162.0 (Cq), 196.0 (CO).^{19}F NMR (376.3 MHz, CD_3CN, +25 °C): δ −61.61 (s). HRMS (ESI-TOF-MS^+) m/z: $[M + H]^+$ calcd for $C_{28}H_{21}F_3N_3O_2$: 488.15859; found: 488.15805.

(3-Methyl-1-phenyl-4-(*p*-tolyl)-6-(trifluoromethyl)-1*H*-pyrazolo[3,4-*b*]pyridine-5-yl)(phenyl)methanone (2).[31] Yield: 372 mg (79%, relative to *p*-methylbenzaldehyde). White solid, mp 155−156 °C. ^{1}H NMR (600 MHz, CD_3CN, +50 °C) δ: 2.05 (s, 3H, CH_3), 2.32 (s, 3H, CH_3), 7.14 (br, 4H, Ar−H), 7.38 (t, J = 8.3 Hz, 7.6 Hz, 2H), 7.42 (tt, J = 7.5 Hz, 1.2 Hz, 1H), 7.55 (tt, J = 7.4 Hz, 1.2 Hz, 1H), 7.63 (m, 4H), 8.31 (m, 2H). ^{13}C NMR (150.8 MHz, CD_3CN, +50 °C) δ: 15.3 (CH_3), 21.8 (CH_3) 122.6 (CH), 123.5 (q, J = 275.1 Hz, CF_3) 128.1 (CH), 128.7 (Cq), 130.0 (CH, br), 130.1 (CH), 130.9(CH), 131.0 (CH), 131.2(CH, br), 131.9 (Cq), 135.4 (CH), 139.3 (Cq), 140.6 (Cq), 140.9 (Cq), 144.1 (J = 34.5 Hz, C-CF_3), 145.7 (Cq), 148.0 (Cq), 150.6 (Cq), 195.8 (CO). ^{19}F NMR (376.3 MHz, CD_3CN, +25 °C): δ −61.61. HRMS (ESI-TOF-MS^+) m/z: [M

dx.doi.org/10.1021/jo502047n | J. Org. Chem. 2014, 79, 11039−11050

+ H]$^+$ calcd for $C_{28}H_{21}F_3N_3O$ (M + H)$^+$: 472.16367. found: 472.16116.

(4-(3-Ethylphenyl)-(3-methyl-1-phenyl-6-(trifluoromethyl)-1*H*-pyrazolo[3,4-*b*]pyridine-5-yl)(phenyl)methanone (3). Yield: 266 mg (55%, relative to *m*-ethylbenzaldehyde). White solid, mp 101−102 °C. ^{1}H NMR (600 MHz, CD_3CN, +50 °C): δ 1.07 (bs, 3H), 2.07 (bs, 3H), 2.54 (bs, 2H), 7.03−7.09 (m, 2H), 7.16−7.26 (m, 2H) 7.36 (t, J = 7.6 Hz, 2H), 7.43 (t, J = 7.6 Hz, 1H), 7.54 (t, J = 7.6 Hz, 1H), 7.60−7.65 (m, 4H), 8.32 (d, J = 7.6 Hz, 2H). ^{13}C NMR (150.8 MHz, CD_3CN, +50 °C): δ 15.3 (CH_3), 16.4 (CH_3), 29.8 (CH_2), 122.6 (2 CH), 123.4 (q, J = 275.0 Hz, CF_3), 128.1 (CH), 128.5 (CH), 129.5 (CH), 130.0 (2 CH), 130.1 (CH), 130.8 (CH), 130.9 (2 CH), 131.0 (2 CH), 131.1 (Cq), 134.9 (Cq), 135.3 (CH), 139.3 (Cq), 140.6 (Cq), 144.2 (q, J = 34.4 Hz, *C*-CF_3), 145.7 (Cq), 145.8 (Cq), 148.1 (Cq), 150.6 (Cq), 195.8 (CO). ^{19}F NMR (376.3 MHz, CD_3CN, +25 °C): δ −61.42 (s). HRMS (ESI-TOF-MS$^+$): m/z: [M + H]$^+$ calcd for $C_{29}H_{23}F_3N_3O$: 486.17932; found: 486.17912. Crystals suitable for X-ray analysis (colorless bricks) were obtained by slow evaporation of a hexane/ethyl acetate 4:1 v:v solution.

(4-(3-Isopropylphenyl)-3-methyl-1-phenyl-6-(trifluoromethyl)-1*H*-pyrazolo[3,4-*b*]pyridine-5-yl)(phenyl)methanone (4). Yield: 255 mg (51%, relative to *m*-isopropylbenzaldehyde). White solid, mp 119−120 °C. ^{1}H NMR (600 MHz, CD_3CN, +50 °C): δ 1.07 (bs, 3H), 1.11 (bs, 3H), 2.07 (s, 3H), 2.80 (bs, 1H), 7.05 (d, J = 7.4 Hz, 1H), 7.09 (bs, 1H), 7.20 (d, J = 7.4 Hz, 1H), 7.32 (bs, 1H), 7.36 (t, J = 7.5 Hz, 2H), 7.42 (t, J = 7.5 Hz, 1H), 7.42 (t, J = 7.5 Hz, 1H), 7.61 (d, J = 7.5 Hz, 2H), 7.63 (t, J = 7.8 Hz, 2H), 8.32 (d, J = 8.2 Hz, 2H) ppm. ^{13}C NMR (150.8 MHz, CD_3CN, +50 °C): δ 15.2 (CH_3), 24.4 (CH_3), 24.7 (CH_3), 35.3(CH), 118.6 (Cq), 122.6 (CH), 123.4 (q, J = 275.2 Hz, CF_3), 128.1 (CH), 128.7 (CH), 128.7 (Cq), 128.8 (CH), 129.3 (CH), 129.5 (CH), 130.0 (CH), 130.9 (CH), 131.0 (CH), 134.8 (Cq), 135.3 (CH), 139.3 (Cq), 140.6 (Cq), 144.2 (q, J = 34.4 Hz, *C*-CF_3), 145.7 (Cq), 148.2 (Cq), 150.3 (Cq), 150.6 (Cq), 195.8 (CO) ppm. ^{19}F NMR (376.3 MHz, CD_3CN, +25 °C): δ −61.60 (s). HRMS (ESI-TOF-MS$^+$): m/z: [M + H]$^+$ calcd for $C_{30}H_{25}F_3N_3O$: 500.19497; found: 500.19449.

(4-(3-Isopropylphenyl)-3-methyl-1-phenyl-6-(trifluoromethyl)-1*H*-pyrazolo[3,4-*b*]pyridine-5-yl)(3,5-dimethylphenyl)-methanone (5). Yield: 29 mg, 28%, relative to *m*-isopropylbenzaldehyde). Waxy solid. ^{1}H NMR (600 MHz, CD_3CN, +50 °C): δ 1.00−1.18 (bs, 6H), 2.05−2.08 (bs, 6H), 2.24 (s, 3H), 2.82 (bs, 1H), 7.06 (d, J = 7.6 Hz, 1H), 7.09 (bs, 1H), 7.18 (s, 1H), 7.20−7.28 (m, 4H), 7.43 (t, J = 7.5 Hz, 1H), 7.64 (t, J = 8.0, 2H), 8.33 (d, J = 8.2 Hz, 2H). ^{13}C NMR (150.8 MHz, CD_3CN, +50 °C): δ 15.2 (CH_3), 21.6 (CH_3), 24.4 (CH_3), 24.6 (CH_3), 35.3 (CH), 122.6 (CH), 123.5 (q, J = 275 Hz, CF_3), 128.1 (CH), 128.7 (CH), 128.8 (CH), 129.1 (Cq), 129.2 (CH) 129.4 (CH), 130.9 (CH), 135.0 (Cq), 136.8 (CH), 139.5 (Cq), 140.0 (Cq), 140.6 (Cq), 144.2 (q, J = 35.1 Hz, *C*-CF_3), 145.7 (Cq), 148.1 (Cq), 150.2 (Cq), 150.6 (Cq), 196.0 (CO).^{19}F NMR (376.3 MHz, CD_3CN,+25 °C): δ −61.60 (s). HRMS (ESI-TOF-MS$^+$): m/z: [M + H]$^+$ calcd for $C_{32}H_{29}F_3N_3O$: 528.22627; found: 528.22702.

(3-Methyl-4-(1-naphthyl)-1-phenyl-6-(trifluoromethyl)-1*H*-pyrazolo[3,4-*b*]pyridine-5-yl)(phenyl)methanone (6). Yield: 131 mg (36%, relative to 1-naphthaldehyde). White solid, mp 185−187 °C. ^{1}H NMR (600 MHz, CD_3CN, +50 °C): δ 1.60 (s, 3H), 7.21 (bs, 2H), 7.30 (d, J = 6.5 Hz, 1H), 7.35−7.47 (m, 5H), 7.50 (t, J = 7.6 Hz, 1H), 7.55 (d, J = 7.7 Hz, 2H), 7.65 (t, J = 7.9 Hz, 2H), 7.88 (d, J = 8.4 Hz, 1H), 7.90 (d, J = 8.4 Hz, 1H), 8.34 (d, J = 8.4 Hz, 2H). ^{13}C NMR (150.8 MHz, CD_3CN, +50 °C): δ 14.1 (CH_3), 119.7 (CH), 122.7 (CH), 123.5 (q, J = 275.1 Hz, CF_3), 126.2 (CH), 127.4 (CH), 128.0 (CH), 128.2 (CH), 128.4 (CH), 129.6, 129.7 (CH), 129.8 (CH), 129.9 (bs, CH), 130.7 (CH), 130.9 (CH), 131.2 (CH), 132.2, 133.2, 134.6, 135.1 (CH), 138.9, 140.6, 144.8 (q, J = 34.4 Hz, *C*-CF_3), 145.5, 146.2, 150.6, 195.6 (CO). ^{19}F NMR (376.3 MHz, CD_3CN, +25 °C): δ −61.40 (s). HRMS (ESI-TOF-MS$^+$): m/z: [M + H]$^+$ calcd for $C_{31}H_{21}F_3N_3O$ 508.16367; found: 508.16539. HPLC resolution of the atropisomeric pair: Daicel ChiralPak AD-H (5 μm, 250 × 20 mm), 18 mL/min flow rate, 254 nm detection, +25 °C; eluent: hexane:2-propanol 98:2 v:v; t_R 6.10 and 6.83 min. Crystals of the racemic mixture suitable for X-ray analysis (colorless sticks) were obtained by slow evaporation of a CH_3OH/CH_2Cl_2 3:1 v:v solution.

■ ASSOCIATED CONTENT

Supporting Information

Chemical shift calculations for compounds **3**, **4**; VT-NMR spectra of compounds **2**, **3**, **5**, **6**; transition states for compound **3** and for the phenyl rotation of **4**; ground and transition states for naphthalene rotation of compound **6**; UV spectrum of the first eluted atropisomer of **6**; calculated UV spectrum of acetophenone and MO components of the main UV transitions; excitation energies and oscillator strengths for syn and anti conformations of compound **6**, and images of the molecular orbitals involved in the main ECD transitions; simulation of the ECD spectrum of **6** with different basis sets; X-ray details of compound **3** and **6** (CCDC 1021535 and 1021536); computational details of **1**−**6**; ^{1}H, ^{13}C, and ^{19}F NMR and HRMS spectra of **1**−**7**. This material is available free of charge via the Internet at http://pubs.acs.org.

■ AUTHOR INFORMATION

Corresponding Authors

*E-mail: andrea.mazzanti@unibo.it.

*E-mail: subbu.perum@gmail.com.

Notes

The authors declare no competing financial interest.

■ ACKNOWLEDGMENTS

Financial contribution was received by A.M. from the University of Bologna (RFO funds 2011 and 2012). S.P. thanks University Grants Commission, New Delhi, for the award of BSR Faculty Fellowship. J.C.M. thanks MINECO, Spain, for financial support through grant CTQ2102-33272-BQU. Thanks are due to Ms. Beatrice De Nicola for technical assistance in the calculations and NMR simulations. A.M. thanks Prof. Stefano Superchi (University of Basilicata) and Prof. Lodovico Lunazzi for helpful discussions. ALCHEMY Fine Chemicals & Research (Bologna, www.alchemy.it) is gratefully acknowledged for a generous gift of chemicals.

■ REFERENCES

(1) Clough, J. D.; Roberts, J. D. *J. Am. Chem. Soc.* **1976**, *98*, 1018−1020.

(2) (a) Cozzi, F.; Cinquini, M.; Annunziata, R.; Siegel, J. S. *J. Am. Chem. Soc.* **1993**, *115*, 5330−5331. (b) Tumambac, G. E.; Wolf, C. *J. Org. Chem.* **2005**, *70*, 2930−2938.

(3) (a) Cozzi, F.; Ponzini, F.; Annunziata, R.; Cinquini, M.; Siegel, J. S. *Angew. Chem., Int. Ed. Engl.* **1995**, *34*, 1019−1020. (b) Thirsk, C.; Hawkes, G. E.; Kroemer, R. T.; Liedl, K. R.; Loerting, T.; Nasser, R.; Pritchard, R. G.; Steele, M.; Warren, J. E.; Whiting, A. *J. Chem. Soc., Perkin Trans. 2* **2002**, 1510−1519.

(4) (a) Zoltewicz, J. A.; Maier, N. M.; Fabian, W. M. F. *J. Org. Chem.* **1996**, *61*, 7018−7021. (b) Wolf, C.; Ghebremariam, B. T. *Tetrahedron: Asymmetry* **2002**, *13*, 1153−1156.

(5) Lunazzi, L.; Mancinelli, M.; Mazzanti, A. *J. Org. Chem.* **2007**, *72*, 5391−5394 and references quoted therein.

(6) Lunazzi, L.; Mancinelli, M.; Mazzanti, A. *J. Org. Chem.* **2008**, *73*, 2198−2205.

(7) Ben-Efraim, D. A.; Arad-Yellin, R. *J. Chem. Soc., Perkin Trans. 2* **1994**, 853−860.

(8) Lai, Y.-H.; Chen, P. *J. Chem. Soc., Perkin Trans. 2* **1989**, 1665−1670.

(9) Staab, H. A.; Chi, C.-S.; Dabrowski, J. *Tetrahedron* **1982**, *38*, 3499.

(10) Casarini, D.; Lunazzi, L.; Foresti, E.; Macciantelli, D. *J. Org. Chem.* **1994**, *59*, 4637−4641.
(11) Lunazzi, L.; Mazzanti, A.; Munoz Álvarez, A. *J. Org. Chem.* **2000**, *65*, 3200−3206.
(12) Yu, G.; Mason, H. J.; Wu, X.; Wang, J.; Chong, S.; Dorough, G.; Henwood, A.; Pongrac, R.; Seliger, L.; He, B.; Normandin, D.; Adam, L.; Krupinski, J.; Macor, J. *J. Med. Chem.* **2001**, *44*, 1025−1027.
(13) Gunasekaran, P.; Prasanna, P.; Perumal, S. *Tetrahedron Lett.* **2014**, *55*, 329−332 and references cited therein.
(14) Straub, A.; Benet-Buckholtz, J.; Frode, R.; Kern, A.; Kohlsdorfer, C.; Schmitt, P.; Schwarz, T.; Siefert, H. M.; Stasch, J. P. *Bioorg. Med. Chem.* **2002**, *10*, 1711−1717.
(15) Huang, S.; Lin, R.; Yu, Y.; Lu, Y.; Connolly, P. J.; Chiu, G.; Li, S.; Emanuel, S. L.; Middleton, S. A. *Bioorg. Med. Chem. Lett.* **2007**, *17*, 1243−1245.
(16) Saggar, S. A.; Sisko, J. T.; Tucker, T. J.; Tynebor, R. M.; Su, D. S.; Anthony, N. J. (Merck & Co.) *U.S. Patent Appl.* US 2007021442, 2007.
(17) Chiu, G.; Li, S.; Connolly, P. J.; Middleton, S. A.; Emanuel, S. L.; Huang, S.; Lin, R.; Lu, Y. (Janssen Pharmaceutica N.V., Belgium) *PCT Int. Appl.* WO 2006130673, 2006.
(18) Patel, J. B.; Malick, J. B.; Salama, A. I.; Goldberg, M. E. *Pharmacol, Biochem. Behav.* **1985**, *23*, 675−680.
(19) Boerrigter, G.; Burnett, J. C., Jr. *Cardiovasc. Drug Rev.* **2007**, *25*, 30−45.
(20) (a) Sanghvi, Y. S.; Larson, S. B.; Willis, R. C.; Robins, R. K.; Revankar, G. R. *J. Med. Chem.* **1989**, *32*, 945−951. (b) Schmidt, P.; Eichenberger, K.; Wilhelm, M. *Angew. Chem.* **1961**, *73*, 15−22.
(21) Alkorta, I.; Elguero, J.; Roussel, C.; Vanthuyne, N., Piras, P. *Adv. Heterocycl. Chem.* **2012**, *105*, 1−188.
(22) (a) Dos Santos, A. R.; Pinheiro, A. C.; Sodero, A. C. R.; da Cunha, A. S.; Padilha, M. C.; de Sousa, P. M.; Fontes, S. P.; Veloso, M. P.; Fraga, C. A. M. *Quim. Nova* **2007**, *30*, 125−127. (b) Bringmann, G.; Günther, C.; Ochse, M.; Schupp, O.; Tasler, S. *Prog. Chem. Org. Nat. Prod.* **2001**, *82*, 1−293.
(23) Bringmann, G.; Gulder, T.; Gulder, T. A. M.; Breuning, M. *Chem. Rev.* **2011**, *111*, 563−639.
(24) Clayden, J.; La Plante, S. *Angew. Chem., Int. Ed.* **2009**, *48*, 6398−6401.
(25) La Plante, S. *ChemMedChem.* **2011**, *6*, 505−513. La Plante, S. *J. Med. Chem.* **2011**, *54*, 7005−7022.
(26) Zask, A.; Murphy, J.; Ellestad, G. A. *Chirality* **2013**, *25*, 265−274.
(27) For reviews, see (a) Hagmann, W. K. *J. Med. Chem.* **2008**, *51*, 4359−4369. (b) Purser, S.; Moore, P. R.; Swallow, S.; Gouverneur, V. *Chem. Soc. Rev.* **2008**, *37*, 320−330. See also (c) Hiyama, T. *Organofluorine Compounds*; Springer: Berlin, 2000. (d) *Fluorine in Bioorganic Chemistry*; Welch, J. T.; Eswarakrishnan, S., Eds.; Wiley: New York, 1991.
(28) (a) Li, X.; Song, L.; Xing, C.; Zhao, J.; Zhu, S. *Tetrahedron* **2006**, *62*, 2255−2263. (b) Li, D. M.; Song, L. P.; Li, X. F.; Xing, C. H.; Peng, W. M.; Zhu, S. H. *Eur. J. Org. Chem.* **2007**, 3520−3525. (c) Li, D.; Song, L.; Song, S.; Zhu, S. *J. Fluorine Chem.* **2007**, *128*, 952−957.
(29) (a) Atkinson, R. S.; Barker, E.; Edwards, P. J.; Thomson, G. A. *J. Chem. Soc., Perkin Trans. 1* **1995**, 1533−1542. (b) Amii, H.; Kobayashi, T.; Terasawa, H.; Uneyama, K. *Org. Lett.* **2001**, *3*, 3103−3105.
(30) For a review, see (a) Wang, J.; Sańchez-Roselló, M.; Aceña, J. L.; del Pozo, C.; Sorochinsky, A. E.; Fustero, S.; Soloshonok, V. A.; Liu, H. *Chem. Rev.* **2014**, *114*, 2432−2506. See also (b) Frezza, M.; Balestrino, D.; Soulere, L.; Reverchon, S.; Queneau, Y.; Forestier, C.; Doutheau, A. *Eur. J. Org. Chem.* **2006**, 4731−4736. (c) Leroux, F.; Lefebvre, O.; Schlosser, M. *Eur. J. Org. Chem.* **2006**, 3147−3151. (d) Buscemi, S.; Pace, A.; Piccionello, A. P.; Macaluso, G.; Vivona, N. *J. Org. Chem.* **2005**, *70*, 3288−3291.
(31) Gunasekaran, P.; Indumathi, S.; Perumal, S. *RSC Adv.* **2013**, *3*, 8318−8325.
(32) (a) Jennings, W. B. *Chem. Rev.* **1975**, *75*, 307−322. (b) Mislow, K.; Raban, M. *Top. Stereochem.* **1967**, *1*, 1−38.
(33) (a) Testa, B. *Principles of organic stereochemistry*; M. Dekker: New York, 1979; p 87. (b) *IUPAC Compendium of Chemical Terminology*, 2nd ed. (the "Gold Book"); compiled by McNaught, A. D.; Wilkinson, A.; Blackwell Scientific Publications: Oxford, 1997. XML on-line corrected version: http://goldbook.iupac.org (2006−) created by Nic, M.; Jirat, J.; Kosata, B.; updates compiled by Jenkins, B. DOI: 10.1351/goldbook.
(34) It has been pointed out that the calculations of entropy data needed to extract the Gibbs free energy are thwarted by the existence of low-frequency vibrational modes. See Lan, Y.; Houk, K. N. *J. Am. Chem. Soc.* **2010**, *132*, 17921−17927.
(35) ^{13}C NMR taken at +50 °C confirmed the diastereotopicity of the methyl groups.
(36) Drakenberg, T.; Sommer, J. M.; Jost, R. *Magn. Reson. Chem.* **1976**, *8*, 579−581.
(37) The indicated errors refer to the absolute errors due to the uncertainty in the temperature determination. However, the *difference* between the two barriers (0.2 kcal/mol) is realistic because the line-shape simulations are taken on the same spectrum, and the error due to the rate constant determination is below 0.05 kcal/mol.
(38) Peerdeman, A. F.; Van Bommel, A. J.; Bijvoet, J. M. *Nature* **1951**, *168*, 271−271.
(39) The Cu−Kα source is not available at the University of Bologna, and enantiopure crystals cannot be obtained.
(40) Hooft, R. W. W.; Stravera, L. H.; Spek, A. L. *J. Appl. Crystallogr.* **2008**, *41*, 96−103.
(41) For reviews, see (a) Bringmann, G.; Bruhn, T.; Maksimenka, K.; Hemberger, Y. *Eur. J. Org. Chem.* **2009**, 2717−2727. (b) Pescitelli, G.; Di Bari, L.; Berova, N. *Chem. Soc. Rev.* **2011**, *40*, 4603−4625. (c) Mazzanti, A.; Casarini, D. *WIREs Comput. Mol. Sci.* **2012**, *2*, 613−641.
(42) UV absorption and CD data for this chromophore can be found in Rosini, C.; Spada, G. P.; Proni, G.; Masiero, S.; Scamuzzi, S. *J. Am. Chem. Soc.* **1997**, *109*, 506−512.
(43) Kimura, K.; Nagakura, S. *Theor. Chim. Acta* **1965**, *3*, 164−173. These bands were also obtained in the UV calculations of acetophenone with TD-DFT ωB97XD/6-311++G(2d,p)//B3LYP/6-31g(d) level of calculations. See Table S1 and Figure S14 of SI.
(44) In Gaussian 09 the BH&HLYP functional has the form: $0.5*E_X^{HF} + 0.5*E_X^{LSDA} + 0.5*\Delta E_X^{Becke88} + E_C^{LYP}$.
(45) Zhao, Y.; Truhlar, D. G. *Theor. Chem. Acc.* **2008**, *120*, 215−241.
(46) Chai, J.-D.; Head-Gordon, M. *Phys. Chem. Chem. Phys.* **2008**, *10*, 6615−6620.
(47) Iikura, H.; Tsuneda, T.; Yanai, T.; Hirao, K. *J. Chem. Phys.* **2001**, *115*, 3540−3544.
(48) Yanai, T.; Tew, D.; Handy, N. *Chem. Phys. Lett.* **2004**, *393*, 51−57.
(49) Ambrogi, M.; Ciogli, A.; Mancinelli, M.; Ranieri, S.; Mazzanti, A. *J. Org. Chem.* **2013**, *78*, 3709−3719 and references cited therein..
(50) Weigend, F.; Ahlrichs, R. *Phys. Chem. Chem. Phys.*, **2005**, *7*, 3297−3305. def2-TZVP basis set coefficients for H, C, N, O were downloaded from https://bse.pnl.gov/bse/portal.
(51) Tomasi, J.; Mennucci, B.; Cammi, R. *Chem. Rev.* **2005**, *105*, 2999−3093.
(52) Berova, N.; Di Bari, L.; Pescitelli, G. *Chem. Soc. Rev.* **2007**, *36*, 914−931.
(53) Reichardt, C. *Solvents and solvent effects in organic chemistry*, 3rd ed.; Wiley-VCH: Weinheim, 2003; pp 348−351.
(54) Büttner, S.; Riahi, A.; Hussain, I.; Yawer, M. A.; Lubbe, M.; Villinger, A.; Reinke, H.; Fischer, C.; Langer, P. *Tetrahedron* **2009**, *65*, 2124−2135.
(55) Siegel, J. S.; Anet, F. A. L. *J. Org. Chem.* **1988**, *53*, 2629−2630.
(56) Stonehouse, J.; Adell, P.; Keeler, J.; Shaka, A. J. *J. Am. Chem. Soc.* **1994**, *116*, 6037−6038.
(57) Kupče, E.; Boyd, J.; Campbell, I. D. *J. Magn. Reson. Ser. B* **1995**, *106*, 300−303.
(58) Brown, J. H.; Bushweller, C. H. *QCPE Bull.* **1983**, *3*, 103−103. A copy of the program is available on request from the authors (A.M.)..

(59) This is usual in the majority of conformational processes investigated by dynamic NMR. For a review, see Casarini, D.; Lunazzi, L.; Mazzanti, A. *Eur. J. Org. Chem.* **2010**, 2035−2056.
(60) Frisch, M. J.; Trucks, G. W.; Schlegel, H. B.; Scuseria, G. E.; Robb, M. A.; Cheeseman, J. R.; Scalmani, G.; Barone, V.; Mennucci, B.; Petersson, G. A.; Nakatsuji, H.; Caricato, M.; Li, X.; Hratchian, H. P.; Izmaylov, A. F.; Bloino, J.; Zheng, G.; Sonnenberg, J. L.; Hada, M.; Ehara, M.; Toyota, K.; Fukuda, R.; Hasegawa, J.; Ishida, M.; Nakajima, T.; Honda, Y.; Kitao, O.; Nakai, H.; Vreven, T.; Montgomery, Jr., J. A.; Peralta, J. E.; Ogliaro, F.; Bearpark, M.; Heyd, J. J.; Brothers, E.; Kudin, K. N.; Staroverov, V. N.; Kobayashi, R.; Normand, J.; Raghavachari, K.; Rendell, A.; Burant, J. C.; Iyengar, S. S.; Tomasi, J.; Cossi, M.; Rega, N.; Millam, N. J.; Klene, M.; Knox, J. E.; Cross, J. B.; Bakken, V.; Adamo, C.; Jaramillo, J.; Gomperts, R.; Stratmann, R. E.; Yazyev, O.; Austin, A. J.; Cammi, R.; Pomelli, C.; Ochterski, J. W.; Martin, R. L.; Morokuma, K.; Zakrzewski, V. G.; Voth, G. A.; Salvador, P.; Dannenberg, J. J.; Dapprich, S.; Daniels, A. D.; Farkas, O.; Foresman, J. B.; Ortiz, J. V.; Cioslowski, J.; Fox, D. J. *Gaussian 09, rev A.02*; Gaussian, Inc., Wallingford, CT, 2009.
(61) (a) Lee, C.; Yang, W.; Parr, R. G. *Phys. Rev. B* **1988**, *37*, 785−789. (b) Becke, A. D. *J. Chem. Phys.* **1993**, *98*, 5648−5652. (c) Stephens, P. J.; Devlin, F.J.; Chabalowski, C. F.; Frisch, M. J. *J. Phys. Chem.* **1994**, *98*, 11623−11627.
(62) *GaussView 5.0.9*; Gaussian, Inc., Wallingford, CT, 2009.